WILEY-VCH

REPRINT

Channelrhodopsin

Early Formation of the Ion-Conducting Pore in Channelrhodopsin-2
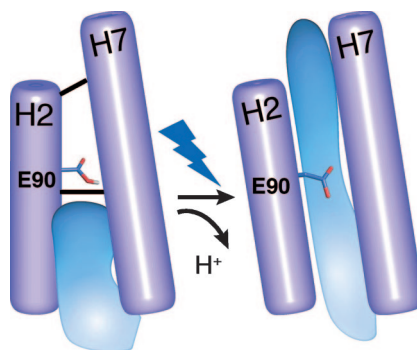
Pore preformation of the ion-conducting channelrhodopsin-2 is triggered by downward movement of the highly conserved E90. Upon light-induced isomerization, the retinal E90 undergoes a conformational change and deprotonation, which leads to water influx and Helix 2 movement.

J. Kuhne, K. Eisenhauer, E. Ritter, P. Hegemann,* K. Gerwert,* F. Bartl ———— **4953 – 4957**

H7

H2

H7

H2

E90

E90

Retinal

-R

H+

1718 cm⁻¹ (E90)
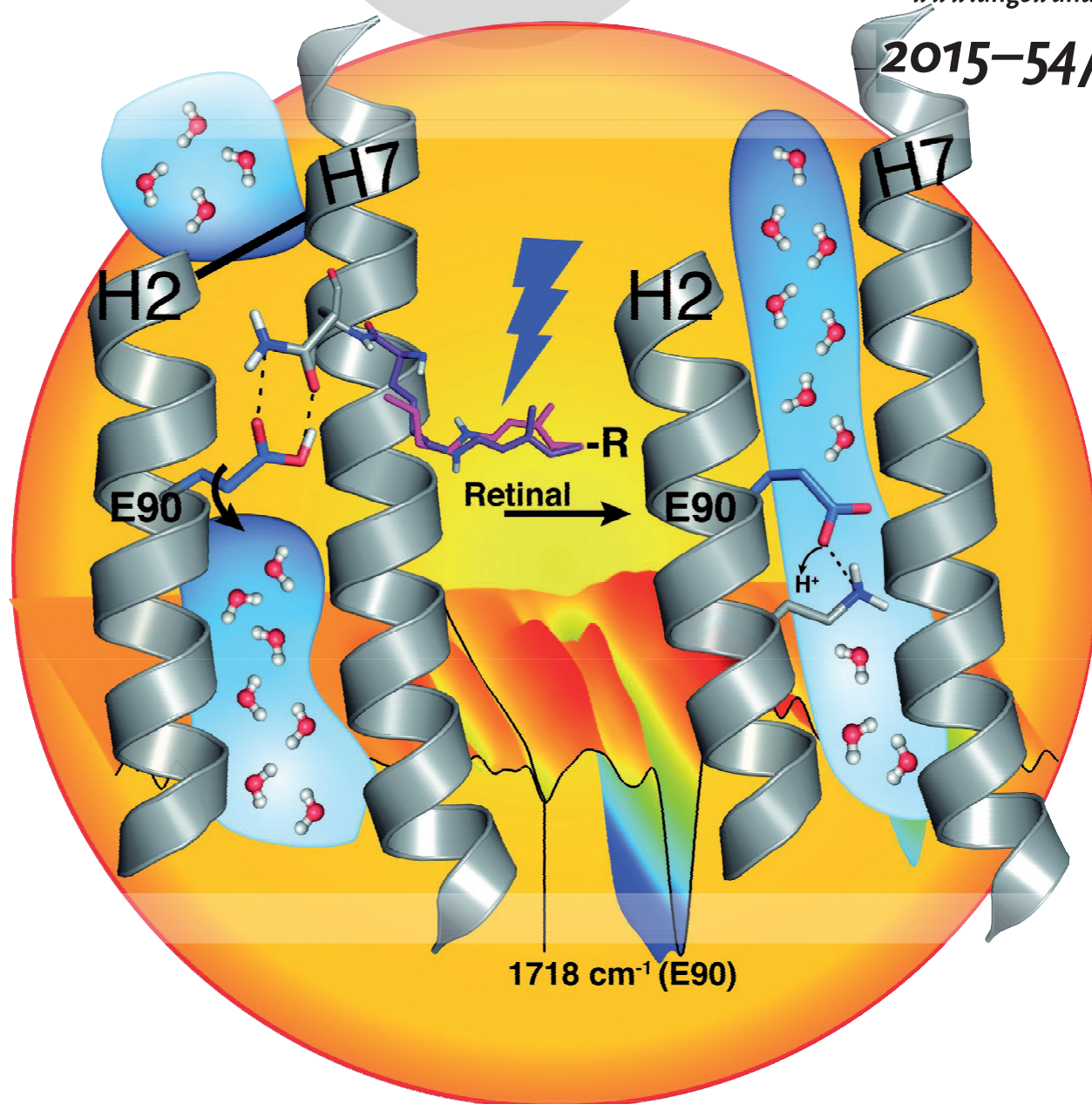
The light-gated ion channel ...

… channelrhodopsin-2 (ChR₂) is the key protein in optogenetics. In their Communication on page 4953 ff., K. Gerwert et al. elucidate channel opening at a molecular level by a combination of time-resolved FTIR spectroscopy and molecular dynamics simulations.

Channelrhodopsin

Early Formation of the Ion-Conducting Pore in Channelrhodopsin-2**

Jens Kuhne, Kirstin Eisenhauer, Eglof Ritter, Peter Hegemann,* Klaus Gerwert,* and Franz Bartl

Abstract: *Channelrhodopsins (ChRs) are light-gated ion channels that are widely used in optogenetics. They allow precise control of neuronal activity with light, but a detailed understanding of how the channel is gated and the ions are conducted is still lacking. The recent determination of the X-ray structural model in the closed state marks an important milestone. Herein the open state structure is presented and the early formation of the ion conducting pore is elucidated in atomic detail using time-resolved FTIR spectroscopy. Photo-isomerization of the retinal-chromophore causes a downward movement of the highly conserved E90, which opens the pore. Molecular dynamic (MD) simulations show that water molecules invade through this opened pore, Helix 2 tilts and the channel fully opens within ms. Since E90 is a highly conserved residue, the proposed E90-Helix2-tilt (EHT) model might describe a general activation mechanism and provides a new avenue for further mechanistic studies and engineering.*

Channelrhodopsins (ChRs) are microbial rhodopsins that conduct cations upon illumination.[1] Light excitation causes all-*trans* to 13-*cis* isomerization of the retinal chromophore followed by a cyclic sequence of conformational changes within the protein that are visible as the photocycle intermediates P500, P390, P520, and P480 on timescales ranging from picoseconds to seconds (inset in Figure 1B). After an actinic light flash, the conducting state P520 evolves from P390 with a rise time of 3 ms. By converting into the late photocycle intermediate P480,[2–5] the channel closes within 40 ms. In continuous bright light, most ChR2 molecules are activated directly from P480, but not from the dark-adapted

state D470. The Helix 2 (H2) residues E82, E83, E90, and E101 are all involved in channel conductance and selectivity.[6–11] E90 in particular is part of the ion-conducting pore and an element of the central gate as suggested by time-resolved Fourier transform infrared (FTIR) experiments, electrical measurements, and homology modeling.[12] Replacement of E90 with lysine or arginine converts the cation channel into a chloride channel with a loss of cation conductance.[13]

Herein, a combination of step-scan FTIR spectroscopy, homology modeling, and MD simulations of protein-bound water molecules elucidates the early pore formation. Upon retinal isomerization, the key residue E90 opens the pore at the narrowest point by a flip to the extracellular side and deprotonates. This allows water influx and induces a H2 tilt, which leads to larger opening and water influx from both sides. We introduce here the E90-Helix2-tilt (EHT) model.

In Figure 1, the homology models of ChR2 based on the C1C2 X-ray structural model[1] are shown in the closed (A) and preopen (B) states. Pore preformation is indicated by the dynamics of protein-internal water molecules, which does not necessarily mean that the channel is conductive yet (for details of the homology modeling and MD simulations, see the Supporting Information, Figure S1). Deprotonation of E90 seems to be crucial in the pore preformation as already shown in time-resolved FTIR experiments with ms time-resolution.[12]

We increased the time resolution to nanoseconds by using the step-scan technique.[14,15] We excited wild-type (WT) ChR2 reconstituted in lipid vesicles with a nanosecond laser flash at $\lambda = 470$ nm and recorded IR absorbance changes from 200 ns to 140 s between $\tilde{\nu} = 1800$ cm^{-1} and 1000 cm^{-1} as well as absorbance changes in the visible range at 390 nm and 520 nm. Based on this complete UV/VIS and IR dataset a detailed molecular mechanism over a time range of nine orders of magnitude can be elucidated similar as previously performed for bacteriorhodopsin.[16] Absorbance changes of marker bands covering the dark-adapted photocycle are presented in Figure 2. They indicate protonation changes of the retinal Schiff base (RSB; 1190 cm^{-1}) and selected carboxylic acids (1718, 1728, 1760 cm^{-1}). To compare the protonation changes with the formation of the key photocycle intermediates P390 and P520, UV/Vis absorbance changes are shown for 390 nm and 520 nm. Additionally the absorbance change of the band at 1661 cm^{-1} (blue) assigned to a conformational change[17] or hydration of α-helices[18] is shown.

The instant appearance of the positive band at 1190 cm^{-1} indicates ultrafast retinal isomerization from all-*trans* to 13-*cis*.[4,17,19] The disappearance of the 1190 cm^{-1} band indicates deprotonation of the protonated Schiff base (RSBH$^+$) with 700 ns. Reprotonation of the RSB occurs with 3 ms

[*] J. Kuhne,[+] K. Eisenhauer,[+] Prof. Dr. K. Gerwert
Lehrstuhl für Biophysik, Ruhr Universität Bochum
Universitätsstrasse 150, 44780 Bochum (Germany)
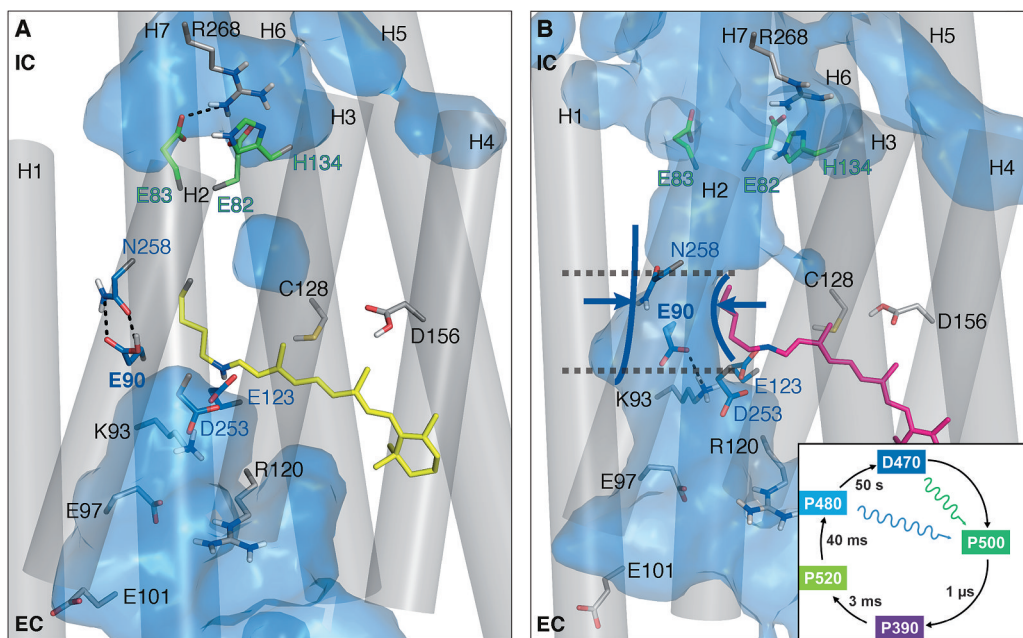E-mail: gerwert@bph.rub.de

Dr. E. Ritter, Prof. Dr. P. Hegemann
Experimentelle Biophysik, Humboldt Universität zu Berlin
Invalidenstrasse 42, 10115 Berlin (Germany)
E-mail: hegemann@rz.hu-berlin.de

Prof. F. Bartl
Institut für Medizinische Physik und Biophysik, Charité
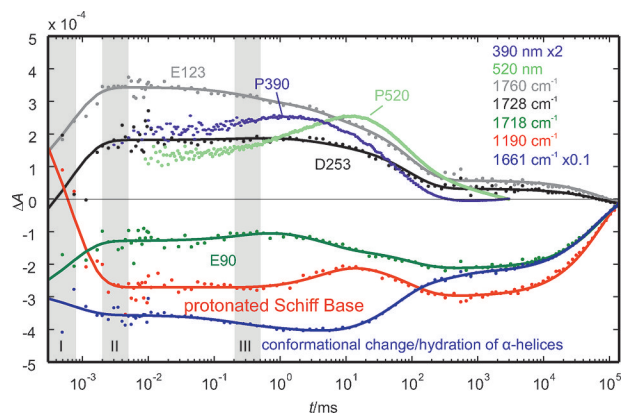Virchovweg 6, 10115 Berlin (Germany)

[+] These authors contributed equally to this work.

Figure 1. ChR2 in A) the dark-adapted (closed) and B) light-adapted (preopen) state. Photocycle of ChR2 (adapted from Ref. [3], halflives obtained from ChR2 reconstituted in lipid vesicles, inset in (B). Water molecule dynamics are indicated as blue surfaces, visualizing the opening of the pore at E90 at the narrowest point. A) Closed dark-adapted state. E90 is inward directed and forms two hydrogen bonds to N258, thereby connecting H2 with H7. E83 is hydrogen-bonded to R268 and connects H2 with H7 additionally on the intracellular side of the protein (IC). Both connections prevent water influx into the intracellular vestibule. B) Preopen light-adapted state. Retinal isomerization causes breakage of the E90-N258 connection, flip of E90 from the inward (IC) to the outward (EC) orientation, and thereby breakage of the connection between H2 and H7. Deprotonated E90 forms a new salt bridge to K93, causing the outward tilt of H2 and invasion of extracellular water. E82 is separated from R268, facilitating the influx of intracellular water and the complete preformation of the channel.

in accordance with the P390 to P520 transition (Figure 2).[3,5] The absorbance changes at 1718, 1760, and 1728 cm^{-1} reflect protonation changes of E90 and the counter ion residues E123 and D253. They are assigned by comparing WT difference spectra with those of the respective mutants E123T (Supporting Information, Figure S9C), D253N (Figure 7 in Ref. [18]), and E90Q[3,12] in which the corresponding bands completely disappear (further details in the Supporting Information, Figure S2). Both E123 and D253 are protonated simultaneously with RSBH$^+$ deprotonation with 700 ns (Figure 2; Supporting Information, Figure S4). These parallel protonation changes indicate that both might serve as RSB proton acceptors in individual ChR2 molecules.[1,8,20,21] Deprotonation of E123 (1760 cm^{-1}) and D253 (1728 cm^{-1}) occurs during channel closure and transition to the P480 intermediate of about 40 ms (Figure 2).

The appearance of both the negative band at 1718 cm^{-1} caused by E90 and the positive isomerization marker band at 1190 cm^{-1} (Figure 2; Supporting Information, Figure S3), are faster than 200 ns and thus not time-resolved. On the early timescale ($< 1 \mu s$), H-bond changes and deprotonation of E90 cannot be distinguished owing to a low signal-to-noise ratio (SNR). However, E90 is clearly deprotonated in the P390 intermediate and thus a long time before channel opening. E90 reprotonates only in the last step during the transition from P480 to the fully dark-adapted state.[12] Thus, deprotonation of E90 is only visible when the photocycle starts from the fully dark-adapted state, but not when it is started from the light-adapted P480.[18] The appearance of the negative band at 1661 cm^{-1} (blue in Figure 2) occurs on a timescale of 0.5 ps and is not time-resolved here either.[17] The bi-phasic decay of this band accompanies pore closure ($t_{1/2} \approx 40$ ms) and dark-state recovery together with E90 reprotonation ($t_{1/2} \approx 48$ s). As the hydratisation of α-helices also contributes to this band,[18] this might indicate that water molecules are leaving the channel simultaneously to E90 reprotonation.

To gain deeper structural insight into the functional role of E90, we employed MD simulations on the improved ChR2

Figure 2. IR and UV/Vis absorbance changes of WT ChR2. Absorbance changes of carbonyl bands of E123 at 1760 cm^{-1} (gray), D253 at 1728 cm^{-1} (black), and E90 at 1718 cm^{-1} (dark green), and the retinal C−C stretching vibration at 1190 cm^{-1} (red), indicating the protonation state changes of these residues, are shown in comparison to the formation of P390 (violet) and P520 (green). The kinetic trace of the band at 1661 cm^{-1} is shown in blue. Gray shaded areas (I–III) correspond to the difference spectra in the Supporting Information, Figure S3. (IR dataset corrected for heat artifact: Figure S4, UV/Vis data set scaled and shifted: Figure S5, continuous lines are the resulting global fit (Supporting Information, Experimental Section Figure S4), which provides high accuracy also at lower SNR regions. Reproducibility is shown in the Supporting Information, Figures S3–S5.

WT homology model based on the chimera C1C2 X-ray structure (Figure 1). This will allow us to discuss the experimental results on the background of the structural model. To extend the structural model of the dark-adapted closed state to a light-induced open state model, we induced retinal C13=C14 double-bond isomerization in 20° rotation steps and fixation of the C12−C13=C14−C15 torsion. This approximation neglects the excited state and single bond distortions. The pre- (all-*trans*) and post-isomerization structures (13-*cis*) of the retinal binding site are shown in Figure 3 A. In the dark-adapted all-*trans* retinal configuration E90 on H2 is connected to N258 on H7 via two hydrogen bonds, which keeps the side chains of E90 and N258 in a fixed conformation, as also suggested for the C1C2 X-ray structure.[1,13] Isomerization around the C13=C14 bond induces a strain that is maximal for a dihedral angle of 60°, and propagates via the side chain of K257 to the adjacent N258. This strain induces movement of the N258 side chain, resulting in reduction of the number of hydrogen bonds between E90 and N258 from two to one.

After the loss of one hydrogen bond E90 becomes conformationally more mobile, and moves outward in the
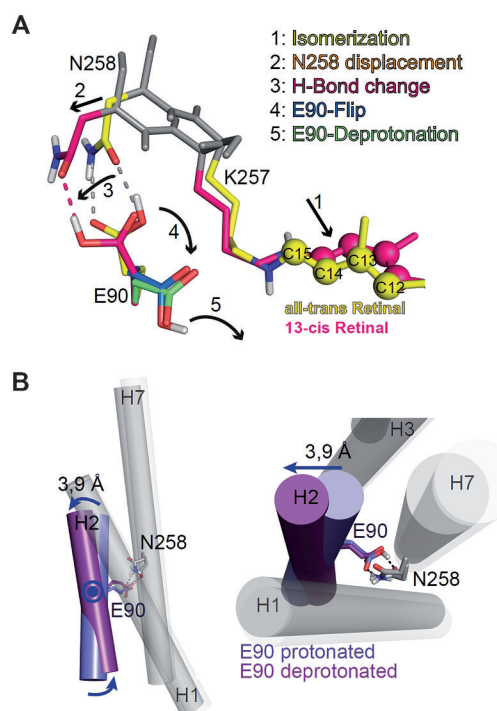
Figure 3. All-*trans* to 13-*cis* isomerization and H2 movement in ChR2 based on MD simulations. A) The side chains are colored and the protein backbone is shown in gray. The all-*trans* and the fully rotated 13-*cis* retinal configurations are shown in yellow and magenta. RSBH$^+$ isomerization (1) is followed by K257 and N258 displacement (2), loss of one hydrogen bond (3), E90 outward flip (4), and E90 deprotonation (5). B) Movement of H2 as a consequence of E90 downward flip and deprotonation. The TM (transmembrane) H2 is colored in lilac for protonated E90 in the inward orientation (up) and in purple for a deprotonated E90 in the outward orientation (down), respectively. Upon the deprotonation and outward flip of E90, H2 is tilted outward by 3.9 Å on the intracellular side of the protein. E90 within H2 functions as a hinge for this movement.

second half of the 100 ns simulation (Figure 3). In the deprotonated form, this outward movement of E90 is even more pronounced in MD simulations, because it is then stabilized by a salt bridge with K93 (Figure 1 B). Comparison of structures before and after retinal isomerization additionally revealed that H2 is tilted outward on the intracellular side by 3.9 Å, with E90 serving as the hinge (Figure 3 B). MD simulations further monitor changes in the distribution of internal water molecules in the preopen state as compared to the closed state (Figure 1 A,B). In the dark-adapted state with all-*trans* RSBH$^+$ (Figure 1 A), water molecules occupy the extracellular half channel (access channel) up to the RSBH$^+$, but the vestibule between the central gate and inner gate is not filled. This is caused by the constrictions at the central gate by E90 and N258 and at the inner gate between E83 and R268, which block the influx of water molecules from the extracellular and intracellular bulk phases, respectively (Figure 1 A). This is also seen in the top view in Figure 4 A. In the
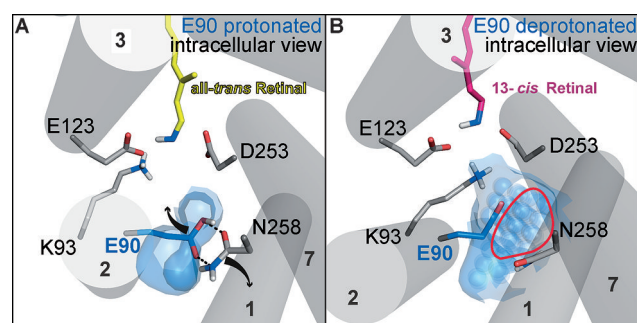
Figure 4. Formation of the water-filled pore upon E90 deprotonation. Water molecule dynamics during the simulation are indicated as blue spheres and lined by surfaces. ChR2 is shown from the intracellular side, water densities are depicted for a 3 Å layer around E90, as indicated in Figure 1 B. A) Closed state (E90 protonated). B) Preopen state: E90 is deprotonated and forms a salt bridge to K93. H2 is tilted outward and the pore between H1, H2, and H7 opens for water invasion. The side chains of E90 and N258 move like a double door: E90 swings downward and N258 swings upward.

simulated preopen structure with 13-*cis* retinal, deprotonated E90 is outward-oriented and forms a salt bridge to K93. This causes also the breakage of the connection between H2 and H7. The resulting outward tilt of H2 on the intracellular side enables water influx from the extracellular side into the vestibule and weakens the salt bridges between E83/R268 and E82/H134 (on H3), which facilitates the influx of water molecules from the intracellular side (Figure 1). Thereby a continuous aqueous pore through the protein, with E90 at the narrowest point is formed (Figure 1 B). This formation of the pore by a "double-door movement" of E90 and N258 is clearly seen in the top view shown in Figure 4. The downward flip and deprotonation of E90 opens the pore and provides open space for water influx.

Because orientation of E90 determines pore formation, we studied how the orientation of E90 in the dark-adapted state might be affected by point mutations and how this explains their electrical properties. Interestingly, for the E90Q

mutant the orientation of Q90 differs from that of protonated E90 in the dark-adapted state, as observed in MD simulations (Supporting Information, Figure S9A). The missing two hydrogen bonds in Q90 to N258 result in higher conformational flexibility. Q90 is with 70 % probability already outward oriented in the dark-adapted state similar like E90 in the deprotonated state after light-activation. This explains now why the Q90 mutant, even it cannot undergo a deprotonation, does only slightly influence the current.

In previous studies, E90 has been replaced by positively charged residues in E90K and E90R,[11–13] which converted the cation selectivity into an anion selectivity (chloride-conducting ChRs, ChloCs).[13] Because lysine as well as arginine are bulky residues, they cannot change their conformation to the inward orientation owing to limited space within the central gate. So, both residues are oriented outward in the dark-adapted state, leading to a more positively charged extracellular vestibule, which is neutralized by an enhanced chloride ion density. Since E90 is a key residue within the central gate, which marks the narrowest point within the conducting pore, it is not surprising that both conductivity and selectivity of the channel are sensitive to structural changes at this position.

The ChR2 mutation E123T, the so called ChETA (ChR2-E123T accelerated) variant, is often used in optogenetic applications where fast action potential firing is requested.[22] In MD simulations, we find in our model for E123T an altered hydrogen-bonding network for the central gate, with E90 already sideward tilted in the dark-adapted state to form a hydrogen bond with D253 instead with N258 as in WT (Supporting Information, Figure S9B). In this orientation, deprotonation of E90 might either be hindered or a high fraction of the ensemble might be deprotonated already in the dark-adapted state. Owing to the observation that the intensity of the E90 band is decreased in the IR difference spectra as shown in the Supporting Information, Figure S9C, we conclude that in the dark-adapted state of E123T the channel is preopened. This might explain the accelerated gating of E123T.

In summary, our findings result in the EHT model: all-*trans* to 13-*cis* isomerization induces the movement of N258, in agreement with the early backbone conformational change at 1661 cm^{-1} observed after a femtosecond flash on a picosecond timescale.[17] The next early events are disruption of H-bonds between N258 and E90, disconnection of H2 and H7, outward flip, and deprotonation of E90. The tilt of H2 in the MD simulations agrees with the light-induced movement of spin-labelled cysteines on H2 and H7, as measured by electron paramagnetic resonance (Supporting Information, Figure S10).[23,24] The outward orientation of E90 opens up a small pore and water molecules invade. The tilt of H2 is accompanied by separation of the salt-bridges E83/R268 and E82/H134 of the inner gate, rather by water influx than deprotonation of E82/E83 (Figure 1 B).

In the EHT model the activation of ChR2 occurs in two major steps. Chromophore isomerization initiates ultra-fast pore preopening by outward movement of E90. In a second later step, which is not completely understood yet, inner gate opening connects the preformed pore from the extracellular side also to the inner bulk phase rendering the pore fully preformed. Because E90 is highly conserved in ChRs[25] the proposed EHT model might describe a general channel activation mechanism (Supporting Information, Table S1).

We have presented a new road in engineering optogenetic tools. We propose that biophysical properties such as ion selectivity, conductivity, and gating kinetics that are important parameters in optogenetic applications are tunable by modifications of the key residues E90, E82, and E83, whereas color tuning can be handled almost independently by modification of the retinal binding pocket, especially by the counterions E123 and D253.

[1] H. E. Kato, F. Zhang, O. Yizhar, C. Ramakrishnan, T. Nishizawa, K. Hirata, J. Ito, Y. Aita, T. Tsukazaki, S. Hayashi, et al., *Nature* **2012**, *482*, 369–374.

[2] P. Berthold, S. P. Tsunoda, O. P. Ernst, W. Mages, D. Gradmann, P. Hegemann, *Plant Cell Online* **2008**, *20*, 1665–1677.

[3] E. Ritter, K. Stehfest, A. Berndt, P. Hegemann, F. J. Bartl, *J. Biol. Chem.* **2008**, *283*, 35033–35041.

[4] M.-K. Verhoefen, C. Bamann, R. Blöcher, U. Förster, E. Bamberg, J. Wachtveitl, *ChemPhysChem* **2010**, *11*, 3113–3122.

[5] C. Bamann, T. Kirsch, G. Nagel, E. Bamberg, *J. Mol. Biol.* **2008**, *375*, 686–694.

[6] Y. Sugiyama, H. Wang, T. Hikima, M. Sato, J. Kuroda, T. Takahashi, T. Ishizuka, H. Yawo, *Photochemical & Photobiological Sciences* **2009**, *8*, 328–336; Photobiological Sciences **2009**, 8, 328–336.

[7] S. Tanimoto, Y. Sugiyama, T. Takahashi, T. Ishizuka, H. Yawo, *Neurosci. Res.* **2013**, *75*, 13–22.

[8] H. C. Watanabe, K. Welke, F. Schneider, S. Tsunoda, F. Zhang, K. Deisseroth, P. Hegemann, M. Elstner, *J. Biol. Chem.* **2012**, *287*, 7456–7466.

[9] A. P. Plazzo, N. De Franceschi, F. Da Broi, F. Zonta, M. F. Sanasi, F. Filippini, M. Mongillo, *J. Biol. Chem.* **2012**, *287*, 4818–4825.

[10] D. Gradmann, A. Berndt, F. Schneider, P. Hegemann, *Biophys. J.* **2011**, *101*, 1057–1068.

[11] K. Ruffert, B. Himmel, D. Lall, C. Bamann, E. Bamberg, H. Betz, V. Eulenburg, *Biochem. Biophys. Res. Commun.* **2011**, *410*, 737–743.

[12] K. Eisenhauer, J. Kuhne, E. Ritter, A. Berndt, S. Wolf, E. Freier, F. Bartl, P. Hegemann, K. Gerwert, *J. Biol. Chem.* **2012**, *287*, 6904–6911.

[13] J. Wietek, J. S. Wiegert, N. Adeishvili, F. Schneider, H. Watanabe, S. P. Tsunoda, A. Vogt, M. Elstner, T. G. Oertner, P. Hegemann, *Science* **2014**, *344*, 409–412.

[14] F. Garczarek, K. Gerwert, *Nature* **2006**, *439*, 109–112.

[15] W. Uhmann, A. Becker, C. Taran, F. Siebert, *Appl. Spectrosc.* **1991**, *45*, 390–397.

[16] K. Gerwert, E. Freier, S. Wolf, *Biochim. Biophys. Acta Bioenerg.* **2014**, *1837*, 606–613.

[17] M.-K. Neumann-Verhoefen, K. Neumann, C. Bamann, I. Radu, J. Heberle, E. Bamberg, J. Wachtveitl, *J. Am. Chem. Soc.* **2013**, *135*, 6968–6976.

[18] V. A. Lórenz-Fonfría, T. Resler, N. Krause, M. Nack, M. Gossing, G. F. von Mollard, C. Bamann, E. Bamberg, R. Schlesinger, J. Heberle, *Proc. Natl. Acad. Sci.* **2013**, 201219502.

[19] K. Gerwert, F. Siebert, *EMBO J.* **1986**, *5*, 805–811.

[20] K. Welke, J. S. Frähmcke, H. C. Watanabe, P. Hegemann, M. Elstner, *J. Phys. Chem. B* **2011**, *115*, 15119–15128.

[21] H. C. Watanabe, K. Welke, D. J. Sindhikara, P. Hegemann, M. Elstner, *J. Mol. Biol.* **2013**, *425*, 1795–1814.

[22] L. A. Gunaydin, O. Yizhar, A. Berndt, V. S. Sohal, K. Deisseroth, P. Hegemann, *Nat. Neurosci.* **2010**, *13*, 387–392.

[23] N. Krause, C. Engelhard, J. Heberle, R. Schlesinger, R. Bittl, *FEBS Lett.* **2013**, *587*, 3309–3313.

[24] T. Sattig, C. Rickert, E. Bamberg, H.-J. Steinhoff, C. Bamann, *Angew. Chem. Int. Ed.* **2013**, *52*, 9705–9708; *Angew. Chem.* **2013**, *125*, 9887–9890.

[25] N. C. Klapoetke, Y. Murata, S. S. Kim, S. R. Pulver, A. Birdsey-Benson, Y. K. Cho, T. K. Morimoto, A. S. Chuong, E. J. Carpenter, Z. Tian, et al., *Nat. Methods* **2014**, *11*, 338–346.